OXFORD

Precision Clinical Medicine, 2024, 7: pbae030

DOI: 10.1093/pcmedi/pbae030
Research Article

Comparative analysis of tertiary lymphoid structures for predicting survival of colorectal cancer: a whole-slide images-based study

Ming He,[1,2,‡] Huifen Ye,[2,3,4,‡] Liu Liu,[5,‡] Su Yao,[6] Zhenhui Li,[2,7] Xinjuan Fan,[8,9,10] Lili Feng,[11] Tong Tong,[3,4] Yanfen Cui,[2,12] Xiaotang Yang,[12] Xiaomei Wu,[13] Yun Mao,[5,*] Ke Zhao,[1,2,14,*] Zaiyi Liu[1,2,*]

[1]Department of Radiology, Guangdong Provincial People's Hospital (Guangdong Academy of Medical Sciences), Southern Medical University, Guangzhou 510080, China
[2]Guangdong Provincial Key Laboratory of Artificial Intelligence in Medical Image Analysis and Application, Guangzhou 510080, China
[3]Department of Radiology, Fudan University Shanghai Cancer Center, Shanghai 200032, China
[4]Department of Oncology, Shanghai Medical College, Fudan University, Shanghai 200032, China
[5]Department of Radiology, The First Affiliated Hospital of Chongqing Medical University, Chongqing 400042, China
[6]Department of Pathology, Guangdong Provincial People's Hospital (Guangdong Academy of Medical Sciences), Southern Medical University, Guangzhou 510080, China
[7]Department of Radiology, The Third Affiliated Hospital of Kunming Medical University, Yunnan Cancer Hospital, Yunnan Cancer Center, Kunming 650118, China
[8]Department of Pathology, The First Affiliated Hospital of Zhengzhou University, Zhengzhou 450052, China
[9]Henan Provincial Key Laboratory of Radiation Medicine, The First Affiliated Hospital of Zhengzhou University, Zhengzhou 450052, China
[10]Tianjian Laboratory of Advanced Biomedical Sciences, Zhengzhou University, Zhengzhou 450052, China
[11]Department of Radiology, Sun Yat-sen University Cancer Center, Guangzhou 510060, China
[12]Department of Radiology, Shanxi Cancer Hospital, Shanxi Medical University, Taiyuan 030013, China
[13]Department of Radiology, The Sixth Affiliated Hospital of Sun Yat-sen University, Guangzhou 510655, China
[14]Medical Research Institute, Guangdong Provincial People's Hospital, Guangdong Academy of Medical Sciences, Guangzhou 510080, China
*Corresponding authors: Zaiyi Liu, liuzaiyi@gdph.org.cn; Ke Zhao, zhaoke@gdph.org.cn; Yun Mao, maoyun1979@163.com
‡Ming He, Huifen Ye, and Liu Liu contributed equally to this work.

Abstract

Background: Tertiary lymphoid structures (TLS) are major components in the immune microenvironment, correlating with a favorable prognosis in colorectal cancer. However, the methods used to define and characterize TLS were not united, hindering its clinical application. This study aims to seek a more stable method to characterize TLS and clarify their prognostic value in larger multicenter cohorts.

Methods: A total of 1609 patients from four hospitals and The Cancer Genome Atlas database were analyzed. We quantified the number and maximum length of TLS along the invasive margin of tumor using hematoxylin and eosin-stained whole-slide images (WSIs). Additionally, the length of the invasive margin was determined to calculate the TLS density. The prognostic value of TLS for overall survival was evaluated. In addition, we examined the association between TLS density and immune cell infiltration using immunohistochemistry-stained WSIs. The performance for predicting overall survival was measured using hazard ratios (HR) with 95% confidence intervals (CI).

Results: Among the three TLS quantification methods, TLS density has the strongest discriminative performance. Survival analysis indicated that higher TLS density correlated with better overall survival [HR for high vs. low 0.57 (95% CI 0.42–0.78) in the primary cohort; 0.49 (0.35–0.69) in the validation cohort; 0.35 (0.18–0.67) in TCGA cohort]. A high TLS density was associated with a high level of $CD3^+$ T cell infiltration.

Conclusions: Based on this comparative multicenter analysis, TLS density was identified as a simple, robust, and effective immune prognostic index for colorectal cancer.

Keywords: colorectal cancer; tertiary lymphoid structures; digital pathology; prognosis; immune

Introduction

In colorectal cancer (CRC), intratumoral immune responses play a crucial role in controlling tumor progression [1, 2]. Specifically, the presence of immune infiltrates in tumor lesions is associated with a favorable prognosis. Mounting evidence suggests that the existence of T cells in the tumor parenchyma is correlated with improved survival and response to treatment [3, 4]. A T cell-based cellular and molecular tumor profile predicts survival better than either surgical staging or histologic evaluation for other risk factors [5]. However, in addition to intratumoral immune cells, the accumulation of immune infiltrating cells in the tumor is similarly incredibly critical. Tertiary lymphoid structures (TLS) are such organized aggregates of immune cells that form in non-lymphoid tissues under extensive and chronic stimulation, which are characterized by $CD20^+$ B cell structures surrounded by $CD3^+$ T cells [2, 6]. Similar to secondary lymphoid organs (SLO), TLS are es-

Received 11 September 2024; revised 28 September 2024; accepted 15 October 2024. published 18 October 2024

sential not only for the induction but also for the maintenance of immune responses [2]. TLS are believed to sustain the antitumor response in solid malignancies as the presence of TLS in the context of cancer has been linked with a good prognosis [7–10]. TLS density as well as the presence of their components, such as T follicular helper cells, follicular B cells, and high endothelial venules, have been shown to correlate with better survival in many different tumor types [11–13]. Additionally, given the significance of TLS in immunity, recent studies have also presented evidence for the predictive value of its response to immune checkpoint blockade (ICB). In patients treated with ICBs, the development of TLS is often associated with improved treatment response [14, 15].

Although the prognostic and predictive role of TLS has been suggested in many studies of CRC, the methods used to define and characterize TLS have often varied. Most previous studies used hematoxylin and eosin (HE)-stained slides for TLS evaluation. Graham and Appelman first proposed a qualitative TLS evaluation method, the G–A method [16]. Based on the G–A method, counting the number of lymphoid aggregates (LAs), size-based assessment of LAs, and TLS density measurements have been developed [17–20]. However, different approaches make it difficult to directly compare the value of TLS, hindering the introduction of TLS evaluation in clinical work. A standard and stable method used in pathology laboratories is needed to enable uniform and reliable quantitative detection of TLS in samples, thereby further revealing their predictive and prognostic value in CRC, which is crucial for clinical application.

In this study, we evaluated TLS using three methods in HE-stained whole-slide images (WSIs), and validated and compared its prognostic value in large multicenter cohorts, to seek a more reliable and stable method to characterize TLS and clarify its role in CRC, and to accelerate its clinical application.

Methods

Patient cohorts

This study was ethically approved by the institutional review boards of the four hospitals involved and informed consent was waived because of its retrospective nature. Three cohorts, including a primary, a validation, and The Cancer Genome Atlas (TCGA) cohort, were enrolled. Details of the cohort's composition and the inclusion and exclusion criteria are provided in the online supplementary materials. Patients information including age, sex, tumor location, carcinoembryonic antigen (CEA) level (normal or abnormal using the cutoff value of 5 μg/L), tumor grade (low or high), Tumor-Node-Metastasis (TNM) stage, and microsatellite instability (MSI) status were collected. The clinical endpoint of this study was overall survival (OS). Microsatellite status and consensus molecular subtype (CMS) classifications are provided in the online supplementary materials.

WSI acquisition and TLS assessment

For CRC patients from the primary and validation cohorts, the most invasive part of the primary tumor was selected by pathologists from each center for HE and immunohistochemistry (IHC) staining. One tissue paraffin section of 4–5 μm was selected for HE staining for all the patients. In a subgroup of all patients, another two consecutive tissue paraffin sections were selected for IHC staining ($CD3^+$ and $CD8^+$). The details of the IHC staining procedures were illustrated in our previous study [21]. The procedure of WSI acquisition is given in the online supplementary materials. All slides were manually reviewed by two pathologists, and slides without invasive margin (IM) of tumor determined were excluded for analysis by two pathologists' consensus.

Three quantification methods of TLS were evaluated, including counting the number of LAs (≥3), sized-based assessment of LAs (≥1 mm), and the density of TLS (defined as the number of LAs divided by the length of IM). The invasive front is the interface area between the tumor tissue and the normal tissue and is regarded as the region that manifests tumor aggressiveness [22]. To be specific, an aggregation of lymphocytes ≥100 μm was defined as an LA [18]. Mucosa-associated lymphoid tissue and parts of small lymph nodes were not evaluated as LAs. The total number of LAs (≥3) observed on the HE-stained WSIs lining the tumor invasive front were recorded, as described by Buckowitz *et al.* [17]. The largest LA in each patient was identified and its maximum diameter (≥1 mm) was recorded, as described by Ueno *et al.* [18]. The density of the TLS was defined as the number of LAs divided by the length of the IM, as described by Väyrynen *et al.* [19]. We used a computer-assisted method to annotate LAs and the line of the tumor invasive front in WSIs. A digital slide viewer (ImageScope v12.4.3, Leica, USA) was used to view and annotate WSIs, generating xml files for processing. In-house software based on MATLAB (R2020a, MathWorks, USA) was used to automatically extract the TLS information.

For the inter-observer agreement evaluation, two annotators (M.H. and S.Y.), who were blinded to each other's evaluation results and patient information, quantified the TLS for a randomly selected 100 patients from the primary cohort. Then one of the annotators (M.H.) assessed the TLS for all the patients.

$CD3^+$ and $CD8^+$ T cell density calculation

To explore the relationship between TLS and tumor-infiltrating lymphocytes, we used an artificial intelligence (AI)-based method for image processing on WSIs to quantify the density of $CD3^+$ and $CD8^+$ T cells in the core of the tumor (CT) and the IM regions. At the tissue level, we used a deep learning model to extract tumor and normal tissue regions. The tumor tissue region is defined as the CT region and the IM region. At the cell level, we used algorithms such as super-pixel and watershed to segment $CD3^+$ and $CD8^+$ T cells within the CT or IM. Finally, we obtained six densities of immune cells: CD3-CT ($CD3^+$ T cells in the CT region), CD3-IM ($CD3^+$ T cells in the IM region), CD3 ($CD3^+$ T cells in the tumor tissue region), CD8-CT ($CD8^+$ T cells in the CT region), CD8-IM ($CD8^+$ T cells in the IM region), and CD8 ($CD8^+$ T cells in the tumor tissue region). Details of the AI-based imaging process are presented in our previous study [21].

Statistical analysis

R software (v4.1.2) was used for statistical analysis. Fisher's exact test was performed for comparison of categorical variables and Student's t test was performed for comparison of continuous variables. Inter-observer agreement was evaluated using a Cohen's kappa coefficient with equal weights. Kaplan–Meier analysis with log-rank test was performed for survival differences comparison. The associations between OS and variables were evaluated with multivariable Cox regression models using a stepwise forward method, with $P < 0.05$ as the entry point, for variable selection. A two-sided P value < 0.05 was considered statistically significant.

Results

Patient characteristics and TLS quantification

The overall workflow of this study is present in Fig. 1. A total of 1609 CRC patients were enrolled in this retrospective study. There were 545 (mean age 63.2 ± 12.5 years), 888 (61.0 ± 12.9), and 176 (65.4 ± 12.4) patients in the primary, validation, and TCGA cohorts, respectively. The details of the clinical characteristics of the patients in the three cohorts are presented in supplementary Table S1, see online supplementary material. The median follow-up of survivors was 6.5 (interquartile range 5.5–8.6) years in the primary, 4.0 (3.0–5.1) years in the validation, and 2.2 (1.4–4.7) years in TCGA cohort. Supplementary Figure S1 shows the distribution characteristics of different evaluation methods (TLS number, tumor IM length, TLS max length, and TLS density) of TLS in different centers (supplementary Fig. S1, see online supplementary material).

Supplementary Fig. S2 (see online supplementary material) illustrates examples of TLS in the invasive front. For TLS density, patients were grouped as low and high TLS density according to the cut-off value of 0.28 foliciles/mm determined in the primary cohort (supplementary Fig. S3, see online supplementary material), using maximally selected rank statistics. In the primary cohort, 299 (54.9%) patients were classified as the high TLS density group, 553 (62.3%) patients were classified as high TLS density in the validation cohort, and the high TLS group consisted of 114 (64.8%) patients in TCGA cohort. Clinical and histopathological variables for the three cohorts with high and low TLS density are presented in supplementary Table S2, see online supplementary material.

Inter-observer agreement analysis

Figure 2 shows the results of consistency analysis of 100 patients with CRC randomly selected from the primary cohort. Figure 2A provides a detailed comparison of the results from two pathologists who evaluated 100 CRC patients using three TLS assessment methods, including density, number, and maximum length. All three quantification methods of TLS had good to excellent agreement (kappa values were 0.76 for TLS density, 0.89 for TLS number, and 0.76 for TLS max length, respectively). We also observed that although the number of cases misclassified by TLS number and TLS max length was relatively small, these two methods classified more cases into the TLS low group.

Prognostic value of TLS

For TLS density, patients were grouped as low and high TLS density according to the cut-off value of 0.28 foliciles/mm determined in the primary cohort (supplementary Fig. S3, see online supplementary material), using maximally selected rank statistics. High TLS density was associated with favorable OS in the three cohorts (all $P < 0.05$, Fig. 3). With TLS density increased, the 5-year OS rates increased from 69.4% in the TLS density low group to 81.2% in the TLS density high group in the primary cohort. Similar trends were observed in the validation cohort (70.7–85.5%) and TCGA cohort (44.0–80.2%). Unadjusted hazard ratio (HR) for high vs. low in the primary, validation, and TCGA cohorts was 0.57 [95% confidence interval (CI) 0.42–0.78, $P < 0.001$], 0.49 (0.35–0.69, $P < 0.001$), and 0.35 (0.18–0.67, $P = 0.002$), respectively (Table 1).

However, as to the prognostic value of the TLS number and TLS maximum length, inconsistent results were observed among the three cohorts, as presented in Table 1 and supplementary Fig. S4, see online supplementary material. For TLS number, >3 LAs was associated with favorable OS (primary cohort, $P = 0.026$; validation cohort, $P = 0.0001$, supplementary Fig. S4A, C). However, TLS number had no statistically significant impact on OS in TCGA cohort ($P = 0.100$, Supplementary Fig. S4E). TLS maximum length > 1 mm was associated with unfavorable OS in the validation cohort ($P = 0.022$, supplementary Fig. S4D), while the difference was no longer present in the primary and TCGA cohorts ($P > 0.05$, supplementary Fig. S4B, F).

TLS density as an independent prognostic factor for OS

We performed univariate analyses on age, sex, stage, location, CEA level, grade, TLS density, TLS number, and TLS maximum length. In univariate Cox analyses, characteristics that reached significance for OS were age, TNM stage, CEA level, TLS density, and TLS number (Table 1, all $P < 0.05$) in the primary cohort. In the multivariate analysis in the three cohorts, TLS density was still related to OS, independent of age and TNM stage [primary cohort: adjusted HR for high vs. low 0.57 (95% CI 0.41–0.80), $P = 0.001$; validation cohort: 0.60 (0.42–0.86), 0.006; TCGA cohort: 0.35 (0.18–0.68), 0.002; Table 1].

To evaluate the added prognostic value of TLS density, we developed five Cox models: TLS density, TLS number, TLS maximum length, stage, and stage + TLS density (supplementary Table S3, see online supplementary material). We observed that the prognostic performance of TLS density [C-index: 0.568 (95% CI 0.529–0.608) in the primary cohort] is better than that of TLS number [0.542 (0.503–0.581)] and TLS maximum length [0.516 (0.489–0.544)] in the primary cohort. Similar trends were found in the validation and TCGA cohorts. Besides, the C-index of a combination of TLS density with stage was better than that of stage alone in all three cohorts (0.673 vs. 0.653 in the primary cohort, 0.669 vs. 0.632 in the validation cohort, and 0.692 vs. 0.670 in TCGA cohort), as shown in supplementary Table S3.

Survival analysis of TLS density stratified with TNM stage

In the subgroup analysis, TLS density remained an independent predictor for OS in stages I, II and IV CRC when stratified with TNM stage ($P < 0.05$; Fig. 4). However, TLS density did not show a significant difference on prognosis stratified by stage III for OS ($P > 0.05$; Fig. 4C).

Association between $CD3^+$ and $CD8^+$ T cell density with TLS density

A total of 476 patients' samples with consecutive sections stained with HE and IHC were available for inclusion in the analysis of $CD3^+$ and $CD8^+$ T cell density (Fig. 5A). TLS density was positively correlated with $CD3^+$ and $CD8^+$ density, and all the correlation coefficients were <0.33 (supplementary Fig. S5A, see online supplementary material). The high TLS density group had a significantly higher density of $CD3^+$ T cells in the tumor center (CD3-CT), infiltration margin (CD3-IM), and whole density of $CD3^+$ and $CD8^+$ T cells (all $P < 0.05$, Fig. 5C, D and supplementary Fig. S5B). Supplementary Fig. S6, see online supplementary material, illustrates representative IHC and segmentation images comparing $CD3^+$ and $CD8^+$ T cell density at CT and IM between the low and high TLS density groups. However, no significant difference was observed in the density of $CD8^+$ cells in the tumor center (CD8-CT) or in the infiltrative margin (CD8-IM) between the high and low TLS density groups. Together, these data indicate that high

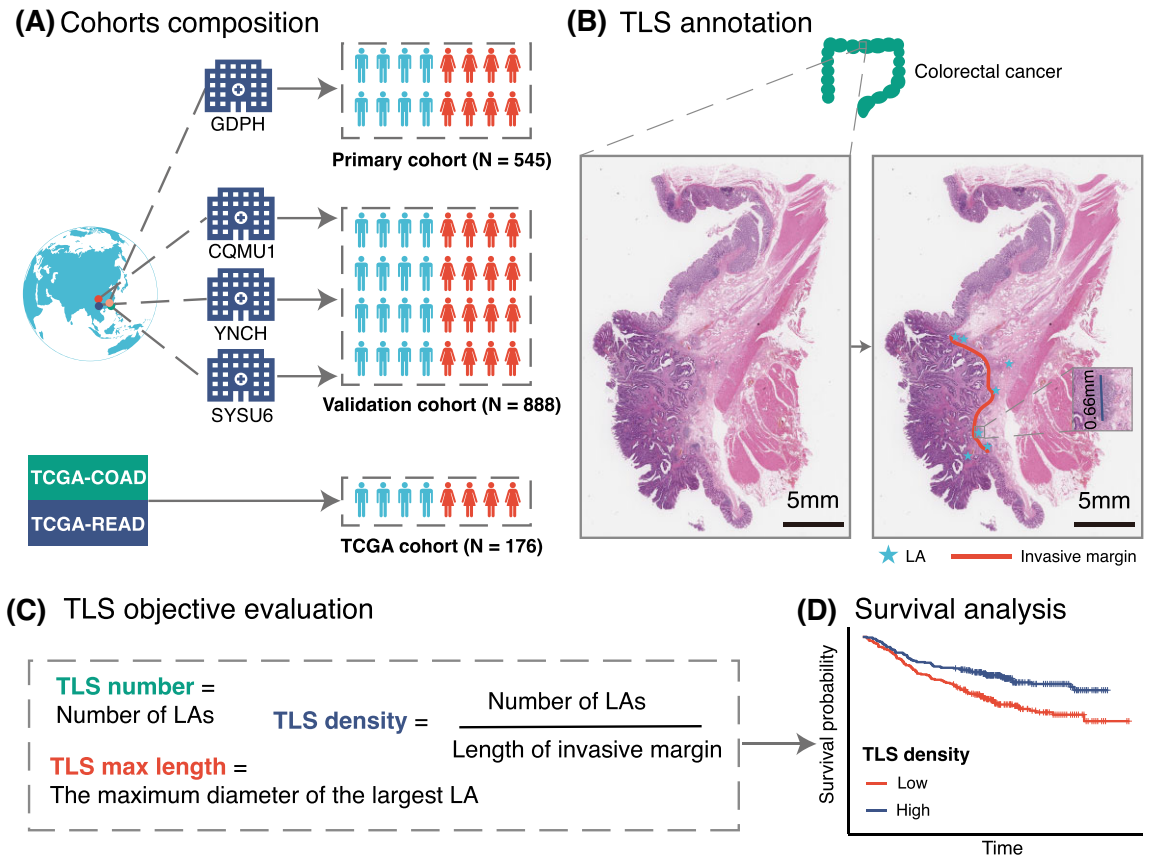

Figure 1. Workflow of the study. (**A**) Cohort composition. (**B**) TLS annotation. (**C**) TLS objective evaluation. (**D**) Survival analysis. TLS, tertiary lymphoid structure.

Table 1. Univariate and multivariate analyses of clinicopathological features and overall survival in whole series (N = 1609).

Variable	Levels	Primary cohort		Validation cohort		TCGA cohort	
		HR (95% CI)	P	HR (95% CI)	P	HR (95% CI)	P
Univariate analysis with Cox model							
Age		1.02 (1.01–1.04)	**<0.001**	1.03 (1.01–1.04)	**<0.001**	1.04 (1.01–1.07)	**0.008**
Sex	Female vs. male	0.92 (0.67–1.27)	0.63	1.03 (0.73–1.45)	0.853	0.63 (0.33–1.22)	0.17
Grade	Low vs. high	1.44 (0.91–2.27)	0.12	0.52 (0.36–0.73)	**<0.001**	NA	NA
Location	Rectum vs. colon	0.97 (0.71–1.33)	0.9	1.50 (1.05–2.15)	**0.025**	1.24 (0.44–3.53)	0.682
Stage	II vs. I	2.28 (1.03–5.07)	**0.043**	1.87 (0.67–5.15)	0.2	0.92 (0.25–3.38)	0.899
	III vs. I	5.61 (2.61–12.1)	**<0.001**	4.97 (1.82–13.6)	**0.002**	1.92 (0.55–6.67)	0.302
	IV vs. I	8.19 (2.97–22.6)	**<0.001**	NA	NA	3.84 (1.04–14.3)	0.044
CEA	Abnormal vs. normal	2.41 (1.75–3.32)	**<0.001**	2.05 (1.45–2.89)	**<0.001**	1.93 (0.71–5.22)	0.195
TLS density	High vs. low	0.57 (0.42–0.78)	**<0.001**	0.49 (0.35–0.69)	**<0.001**	0.35 (0.18–0.67)	**0.002**
TLS number	>3 vs. ≤3	0.70 (0.51–0.96)	**0.027**	0.50 (0.35–0.72)	**<0.001**	0.59 (0.31–1.12)	0.105
TLS max length	>1 mm vs. ≤1mm	0.73 (0.45–1.19)	0.204	0.48 (0.25–0.91)	**<0.001**	0.41 (0.16–1.07)	0.068
Multivariate analysis with Cox model							
Age		1.02 (1.01–1.04)	**0.003**	1.03 (1.01–1.04)	**<0.001**	1.06 (1.02–1.09)	**0.001**
Grade	Low vs. high	NA	NA	0.57 (0.39–0.83)	**0.004**	NA	NA
Location	Rectum vs. colon	NA	NA	2.02 (1.36–3.03)	**0.001**	NA	NA
Stage	II vs. I	2.90 (1.14–7.35)	**0.025**	1.83 (0.65–5.14)	0.249	0.99 (0.26–3.75)	0.991
	III vs. I	5.96 (2.41–14.7)	**<0.001**	3.86 (1.38–10.8)	**0.01**	3.36 (0.94–12.0)	0.062
	IV vs. I	10.6 (3.39–33.3)	**<0.001**	NA	NA	5.62 (1.49–21.2)	**0.011**
CEA	Abnormal vs. normal	1.98 (1.43–2.74)	**<0.001**	1.93 (1.35–2.77)	**<0.001**	NA	NA
TLS density	High vs. low	0.57 (0.41–0.80)	**0.001**	0.60 (0.42–0.86)	**0.006**	0.35 (0.18–0.68)	**0.002**

NA, Not available. *P*-values < 0.05 are shown in bold. CEA, carcinoembryonic antigen; TLS, tertiary lymphoid structure.

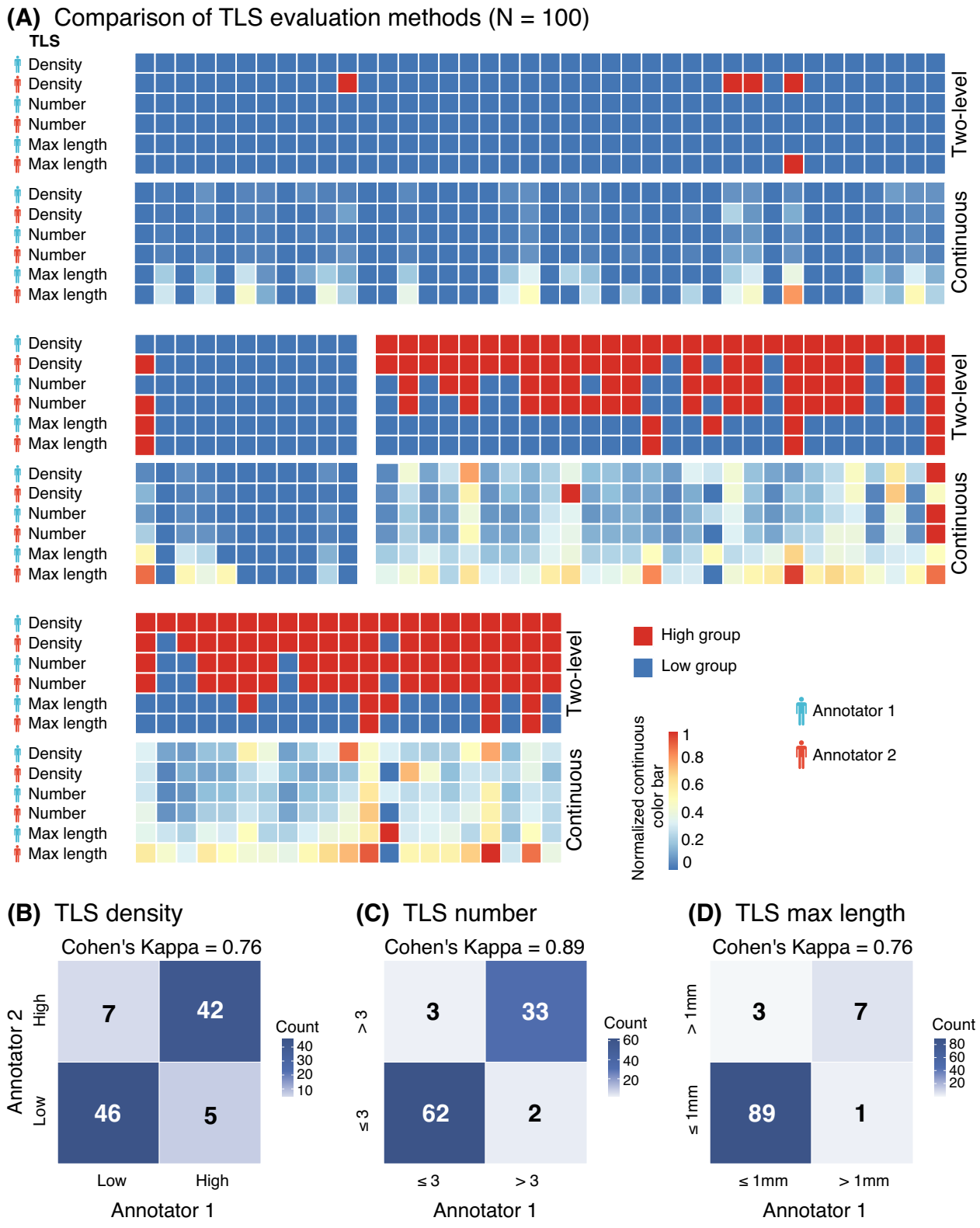

Figure 2. Inter-observer agreement evaluation for the different methods of TLS. (A) Two annotators evaluated 100 cases using three different TLS assessment methods. The three TLS quantifications—TLS density (B), TLS number (C), and TLS maximum length (D)—showed good to excellent inter-observer agreement. TLS, tertiary lymphoid structure.

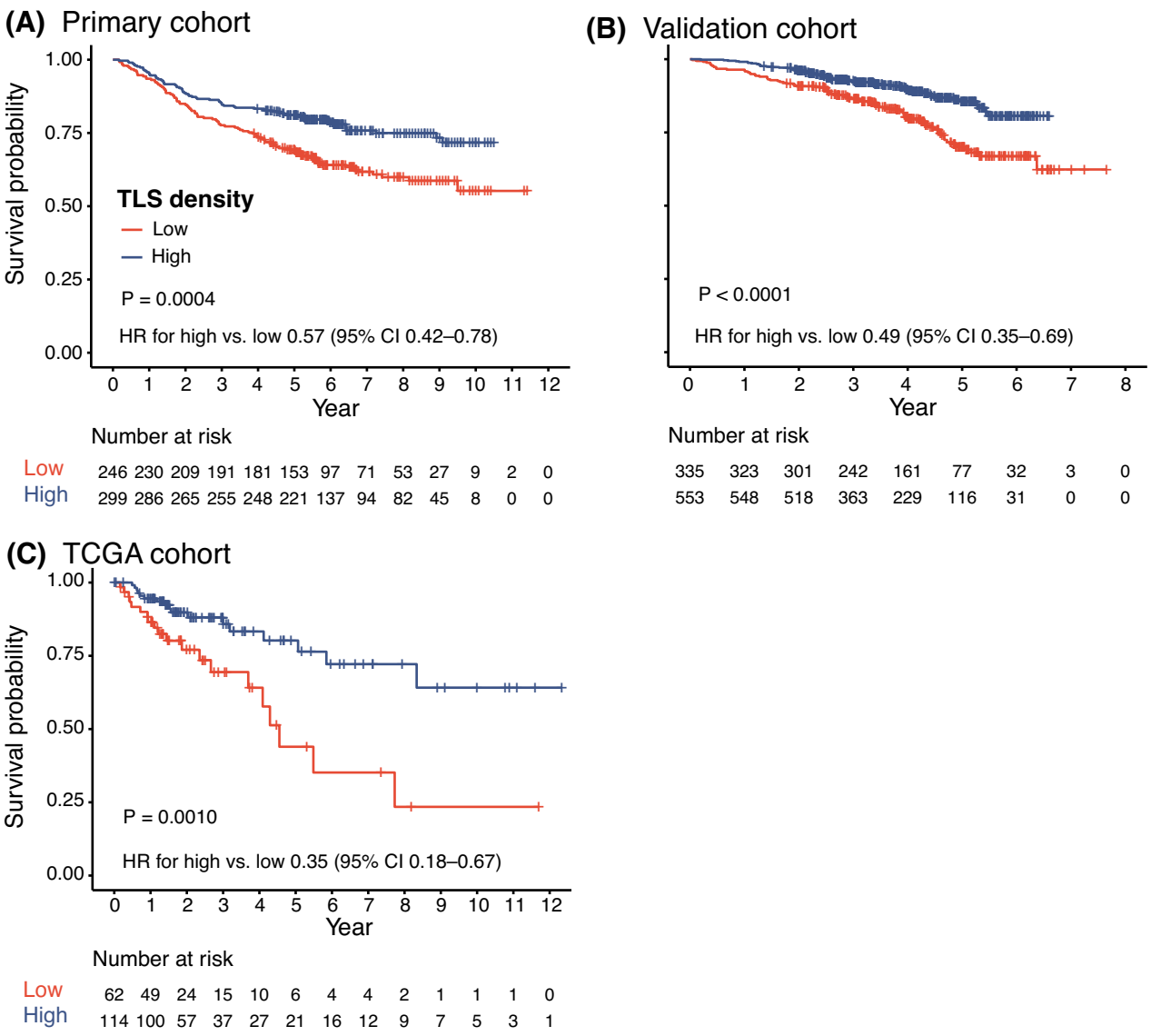

Figure 3. Kaplan–Meier plots for CRC patients according to TLS density. TLS density for OS in the primary cohort (**A**), in the validation cohort (**B**), and in TCGA cohort (**C**). CRC, colorectal cancer; TLS, tertiary lymphoid structure; OS, overall survival; HR, hazard ratio; CI, confidence interval.

TLS density is associated with significantly more T cell infiltration in CRC patients.

Patients with available CD3-stained WSIs were binarized as low and high groups using the median value of density (849.96 number/mm^2) as the cut-off, and the same process was also done for CD8 using the threshold of 411.94 number/mm^2. According to the combination of TLS density and CD3$^+$ T cell density, patients were stratified into four subgroups: low TLS density & low CD3$^+$ density, low TLS density & high CD3$^+$ density, high TLS density & low CD3$^+$ density, high TLS density & high CD3$^+$ density. Survival curves of the four groups are plotted in Fig. 5E. Kaplan–Meier curves show that in the low CD3$^+$ density subgroup, patients with high TLS density have a better OS than patients with low TLS density ($P = 0.001$). As presented in Fig. 5F, we also found that in both high and low CD8$^+$ density subgroups, the category with higher TLS density had a significantly better OS ($P = 0.015$ and 0.012 respectively; Fig. 5F).

Correlation with MSI and CMS subtype

MSI status was detected in 50 (9.2%) cases in the primary, 49 (5.5%) in the validation, and 15 (8.5%) in the TCGA cohort. The percentages of MSI were significantly higher in cases having high TLS density compared with cases having low TLS density in the primary cohort (17.4 vs. 7.4%, $P = 0.005$; Fig. 6A), which is not the case in the TCGA (14.6 vs. 6.3%, $P = 0.246$) or validation (12.2 vs. 11.6%, $P = 0.98$) cohort. CMS classification could be obtained in 99 out of 176 specimens available in TCGA cohort. Frequencies for the available samples were as follows: CMS1 (11.1%), CMS2 (29.3%), CMS3 (21.2%), and CMS4 (38.4%). The pattern of CMS distribution was different between high TLS density (N = 61) and low TLS density (N = 38) groups. While there were comparable frequencies of CMS2 (27.0 vs. 35.0%), CMS3 (22.2 vs. 17.5%), and CMS4 (36.5 vs. 40.0%), noticeable difference of frequencies was observed with regard to CMS1 (14.3 vs. 7.5%; Fig. 6D, E).

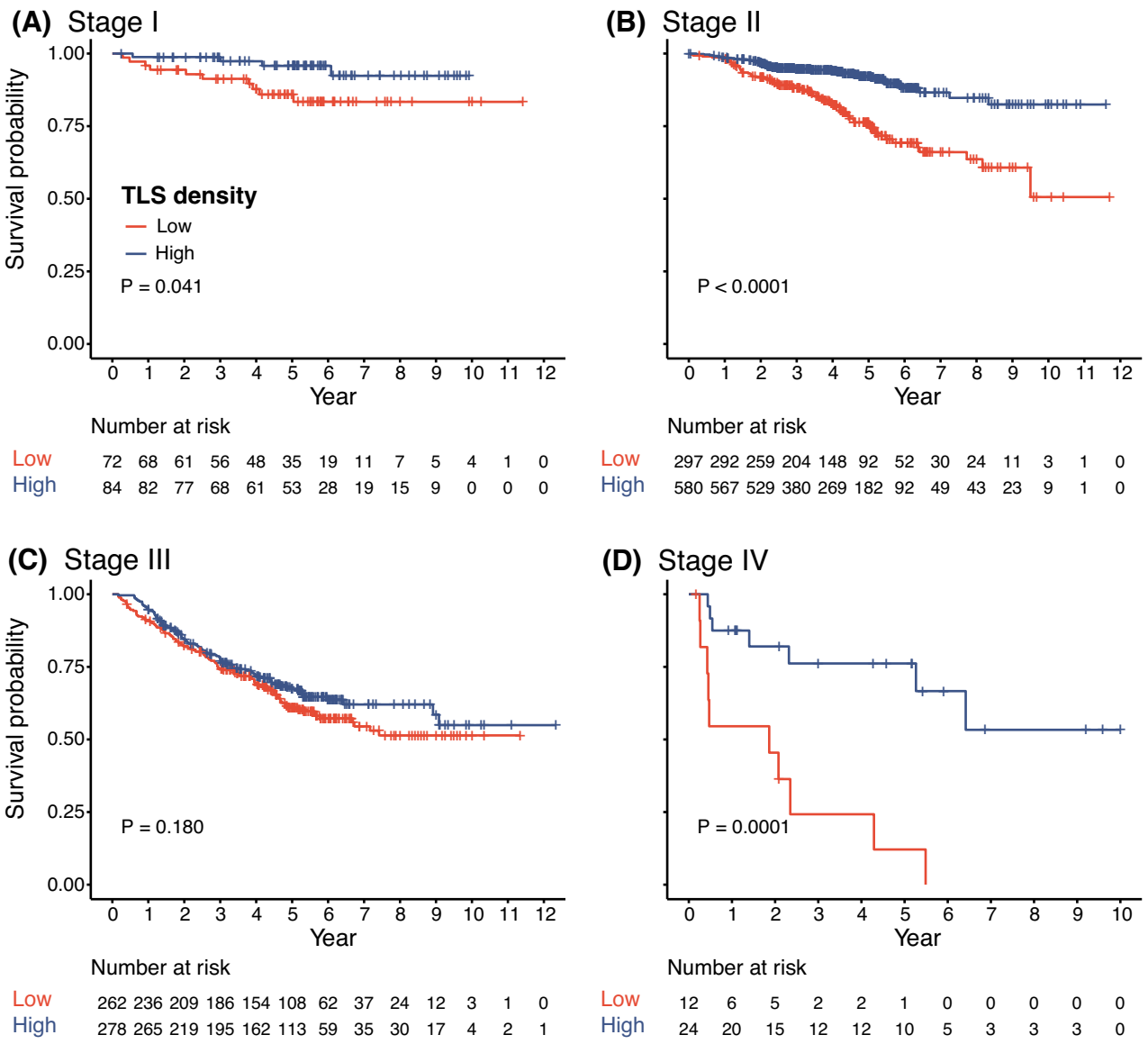

Figure 4. Kaplan-Meier plots for CRC patients stratified with the TNM stage. (**A**) Stage I; (**B**) stage II; (**C**) stage III; and (**D**) stage IV. CRC, colorectal cancer; TLS, tertiary lymphoid structure; TNM, Tumor-Node-Metastasis.

Discussion

TLS are important components of the local microenvironment for cellular and humoral immune responses against tumor cells and have been recognized as indicators of a favorable outcome in almost all solid cancers. However, the methods used to define and characterize TLS were not unified, hindering clinical application. In this study, multicenter data based on a large sample of CRC patients provides compelling evidence that TLS density proved to be an independent prognostic biomarker and outperformed the other methods.

To accelerate the clinical translation of TLS, an objective and robust technique for its presentation was required. WSIs are currently booming in popularity and advances, and considerable information from HE-stained slides has been quantified for many years through digital pathology [23]. The panoramic preview function of WSIs can display the whole lesion, avoiding the defect that only part of the slice could be observed under an ordinary microscope. Additionally, post-processing such as quantitative analysis and labeling of slices can be achieved. Based on the above advantages, WSIs were used to annotate TLS. Besides, although the application of IHC, chromogen, or immunofluorescence is specific and sensitive for reliable identification of TLS [24], TLS detected by IHC represent only a subset of all the TLS which could also be identified on HE-stained slides [25, 26]. Thus, we used a computer-assisted workflow method to quantify TLS on HE-stained WSIs in this study. HE-stained WSIs could identify, record, and quantify TLS with higher accuracy, multi-view, and seamlessness, so the evaluation of TLS is more comprehensive and objective, and the results are easier to repeat, which is more conducive to program automation. Therefore, we speculate that the quantification of TLS on HE-stained WSIs could be better applied to clinical practice.

In stratified analysis of TNM stage, TLS density was thought to be a valuable marker of prognosis in stage II CRC, but not different in stage III, which may suggest that TLS was not associated

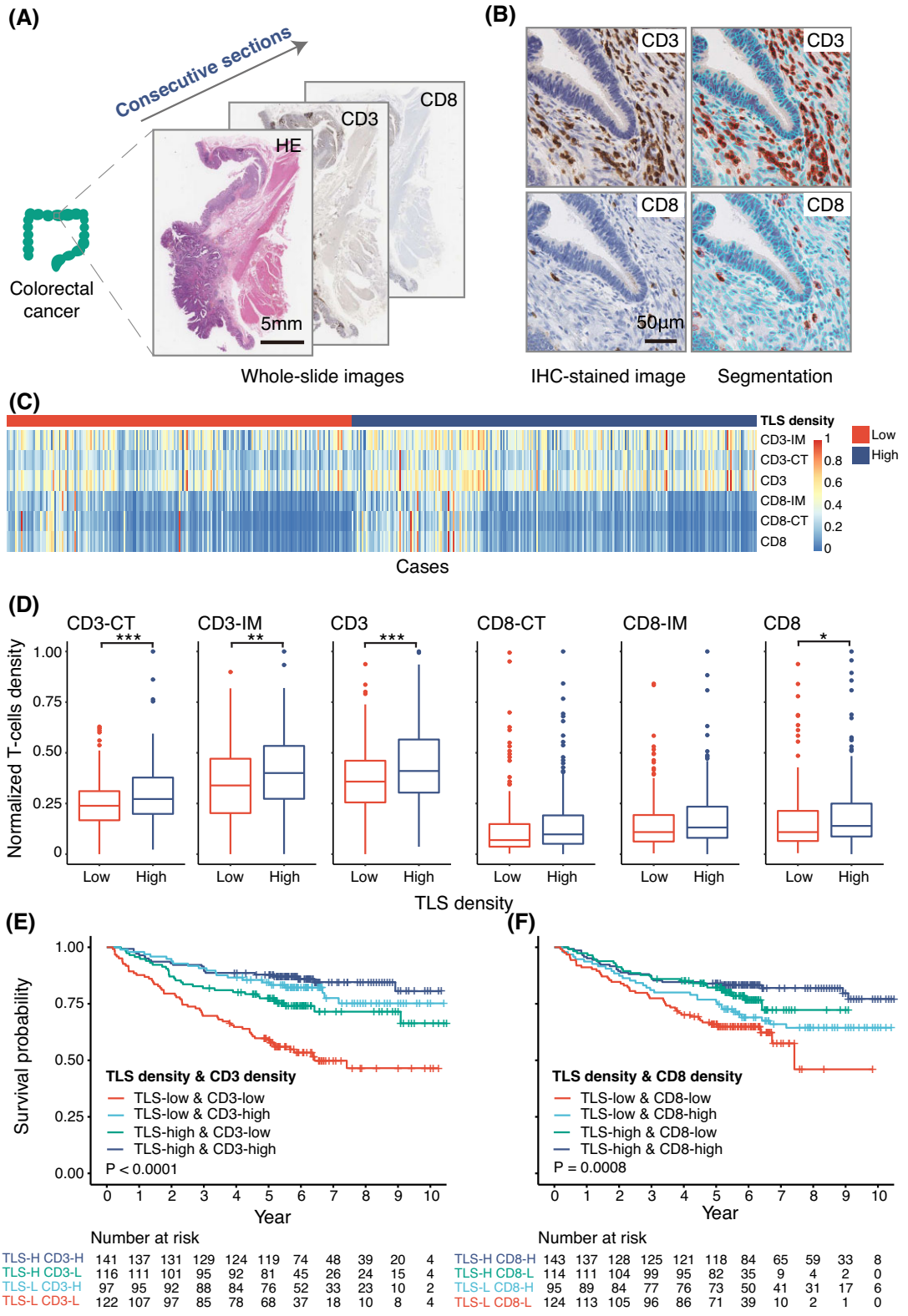

Figure 5. Correlation analysis and survival analysis of CD3$^+$ and CD8$^+$ T cells density and TLS density. (**A**) Consecutive sections. (**B**) Representative staining and segmentation images of CD3$^+$ and CD8$^+$ T cells. (**C**, **D**) Correlation of TLS density with CD3$^+$, CD8$^+$ T cells. (**E**) Kaplan–Meier plots according to TLS density and CD3$^+$ T cells density. (**F**) Kaplan–Meier plots according to TLS density and CD8$^+$ T cells density. TLS, tertiary lymphoid structure; HE, hematoxylin and eosin; IHC, immunohistochemistry; CT, core of tumor; IM, invasive margin.

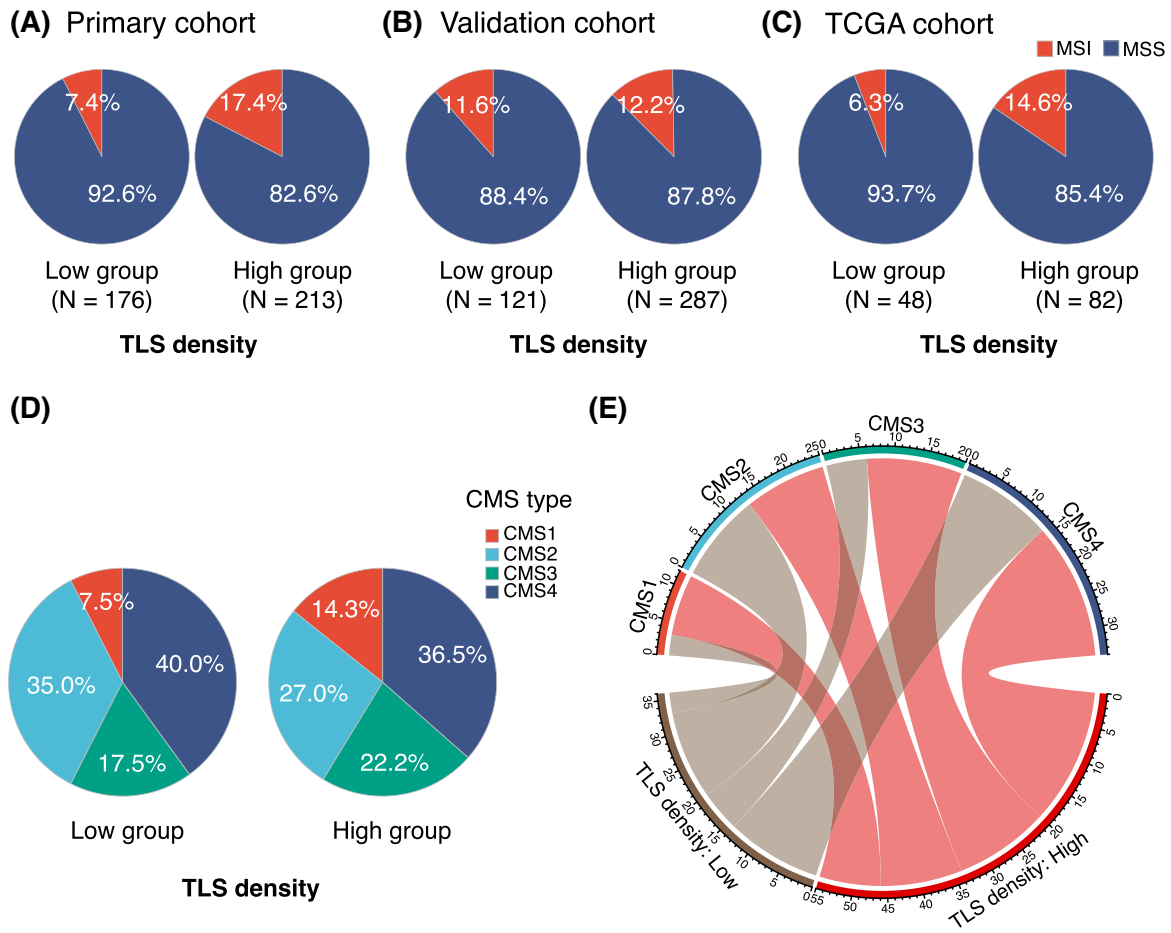

Figure 6. Distribution of MSI, MSS, and CMS in the three cohorts with high and low TLS density. Proportion of MSI and MSS status in the primary cohort (A), validation cohort (B), and TCGA cohort (C). Proportion of CMS among TCGA patients (D, E), stratified by TLS density. MSI, microsatellite instability; MSS, microsatellite stable; CMS, consensus molecular subtype; TLS, tertiary lymphoid structure.

with the prognosis of node-positive CRC. The results were consistent with previous studies [27]. In our study, patients with high TLS density had a favorable prognosis in stage II, indicating that the antitumor effect of immune infiltration was relevant in early stage CRC. The following interpretations may be related. T and B cells within TLS may shorten the time required to generate immune responses by bypassing the need for lymphocyte trafficking to and from SLO [28]. Meanwhile, because of the proximity of TLS to the tumor, lymphocytes may be more likely to encounter cognate antigens, which may facilitate induction of a stronger or broader immune response [2]. However, the prognostic value did not occur in stage III CRC, possibly because lymph node metastases resist T cell-mediated cytotoxicity, induce antigen-specific regulatory T cells, and generate tumor-specific immune tolerance that subsequently facilitates distant tumor colonization [29], or the degree of malignancy and invasion increases with metastasis, limiting the effect of TLS [30]. Overall, these factors weaken the immune effect produced by TLS and have a reduced impact on the prognosis of stage III CRC patients.

Recent studies describing the prognostic value of TLS in cancer have aroused interest in TLS as a potential means of predicting ICB response [31, 32]. MSI status correlated with TLS density and TLS were significantly more prevalent in MSI-high (MSI-H) CRC [33–35]. Presently, many studies have confirmed that ICB was effective in MSI-H CRC. Genetic and epigenetic defects, such as MSI-H, could lead to somatic mutation, increase susceptibility to ICB, and induce the immune escape mechanism of tumor cells, which in turn affects ICB response [36, 37]. The development of TLS was associated with an improved treatment response in patients treated with immune checkpoint inhibitors. Therefore, we speculate that TLS could also predict ICB responses [38, 39]. In this study, we found that MSI status correlated with TLS density, which was consistent with previous studies [33–35]. Currently, our research findings have not directly assessed the relationship between TLS and ICB response, but rather provide a potential link. In the future, we plan to explore the potential predictive value of TLS for ICB response in CRC patients using IHC or multiplex immunofluorescence techniques.

In brief, as to the relationship of TLS with other predictive and/or prognostic biomarkers, high TLS density is positively correlated with mismatch repair deficiency and high peritumoral and intratumoral densities of T cells, suggesting an important role for TLS in adaptive antitumor immunity. TLS density may shed light on personalized treatment for CRCs. Substantial differences in clinicopathological features were observed among the primary, validation, and TCGA cohorts. However, the TLS density-based classifier proposed in this study is of value in stratifying patient prognosis across all three cohorts. This result indicates that the prognostic value of TLS density can hold up in real-world clinical settings.

Despite the considerable strengths of our study, the study has several limitations. One major weakness is that it is a retrospective study. Second, we quantified the TLS but did not make a distinction among different subtypes of all the TLS described by Posch *et al.* previously [33]. A future study is needed to quantify TLS of different subtypes. Third, longitudinal analysis of TLS can reveal changes in density and composition over time, shedding light on their role in treatment response. However, for rectal cancer patients undergoing direct surgery, only biopsy and surgical specimens are available. Specifically, the biopsy samples provide insufficient range for an effective assessment of TLS. Consequently, our research did not explore these temporal changes, highlighting a notable limitation of the study. Finally, our current research was still based on manual evaluation. At present, with the help of AI, many other studies have also performed well [40, 41]. In future work, we hope to use AI to achieve automatic identification and analysis of TLS.

In conclusion, based on this comprehensive multicenter analysis, TLS density was identified as a simple, robust, and effective immune index for resected CRC patients, with potential value in refining risk stratification in clinical practice.

Ethics statement

This study was ethically approved by the institutional review boards of the four hospitals and informed consent was waived because of the retrospective nature of the work.

Acknowledgments

This work was supported by the National Science Fund for Distinguished Young Scholars of China (Grant No. 81925023), Joint Funds of the National Natural Science Foundation of China (Grant No. U23A20478), and the National Science Foundation for Young Scientists of China(Grant No. 82202267, 82101996).

Author contributions

Ming He (Conceptualization, Writing—original draft, Writing—review & editing), Huifen Ye (Conceptualization, Writing—original draft, Writing—review & editing), Liu Liu (Conceptualization, Data curation, Writing—review & editing), Su Yao (Data curation, Writing—review & editing), Zhenhui Li (Data curation, Writing—review & editing), Xinjuan Fan (Data curation), Lili Feng (Writing—review & editing), Tong Tong (Writing—review & editing), Yanfen Cui (Methodology, Writing—review & editing), Xiaotang Yang (Writing—review & editing), Xiaomei Wu (Writing—review & editing), Yun Mao (Writing—review & editing), Ke Zhao (Conceptualization, Funding acquisition, Methodology, Writing—original draft, Writing—review & editing), and Zaiyi Liu (Conceptualization, Funding acquisition, Writing—review & editing)

Supplementary data

data are available at *PCMEDI* online.

Conflict of interest

None declared. As an Editorial Board Member of *Precision Clinical Medicine*, the corresponding author Z.L. was blinded from reviewing and making decisions on this manuscript.

References

1. Galon J, Costes A, Sanchez-Cabo F *et al.* Type, density, and location of immune cells within human colorectal tumors predict clinical outcome. *Science* 2006;**313**:1960–4. https://doi.org/10.1126/science.1129139.
2. Schumacher TN, Thommen DS. Tertiary lymphoid structures in cancer. *Science* 2022;**375**:eabf9419. https://doi.org/10.1126/science.abf9419.
3. Bruni D, Angell HK, Galon J. The immune contexture and Immunoscore in cancer prognosis and therapeutic efficacy. *Nat Rev Cancer* 2020;**20**:662–80. https://doi.org/10.1038/s41568-020-0285-7.
4. Pagès F, Mlecnik B, Marliot F *et al.* International validation of the consensus Immunoscore for the classification of colon cancer: a prognostic and accuracy study. *Lancet North Am Ed* 2018;**391**:2128–39. https://doi.org/10.1016/S0140-6736(18)30789-X.
5. Melero I, Rouzaut A, Motz GT *et al.* T-cell and NK-cell infiltration into solid tumors: a key limiting factor for efficacious cancer immunotherapy. *Cancer Discov* 2014;**4**:522–6. https://doi.org/10.1158/2159-8290.CD-13-0985.
6. Sautès-Fridman C, Petitprez F, Calderaro J *et al.* Tertiary lymphoid structures in the era of cancer immunotherapy. *Nat Rev Cancer* 2019;**19**:307–25. https://doi.org/10.1038/s41568-019-0144-6.
7. Lin Q, Tao P, Wang J *et al.* Tumor-associated tertiary lymphoid structure predicts postoperative outcomes in patients with primary gastrointestinal stromal tumors. *Oncoimmunology* 2020;**9**:1747339. https://doi.org/10.1080/2162402X.2020.1747339.
8. Helmink BA, Reddy SM, Gao J *et al.* B cells and tertiary lymphoid structures promote immunotherapy response. *Nature* 2020;**577**:549–55. https://doi.org/10.1038/s41586-019-1922-8.
9. Calderaro J, Petitprez F, Becht E *et al.* Intra-tumoral tertiary lymphoid structures are associated with a low risk of early recurrence of hepatocellular carcinoma. *J Hepatol* 2019;**70**:58–65. https://doi.org/10.1016/j.jhep.2018.09.003.
10. Lynch KT, Young SJ, Meneveau MO *et al.* Heterogeneity in tertiary lymphoid structure B-cells correlates with patient survival in metastatic melanoma. *J Immunother Cancer* 2021;**9**:e002273. https://doi.org/10.1136/jitc-2020-002273.
11. Siliņa K, Rulle U, Kalniņa Z *et al.* Manipulation of tumour-infiltrating B cells and tertiary lymphoid structures: a novel anti-cancer treatment avenue? *Cancer Immunol Immunother* 2014;**63**:643–62. https://doi.org/10.1007/s00262-014-1544-9.
12. Hiraoka N, Ino Y, Yamazaki-Itoh R *et al.* Intratumoral tertiary lymphoid organ is a favourable prognosticator in patients with pancreatic cancer. *Br J Cancer* 2015;**112**:1782–90. https://doi.org/10.1038/bjc.2015.145.
13. Dieu-Nosjean MC, Antoine M, Danel C *et al.* Long-term survival for patients with non-small-cell lung cancer with intratumoral lymphoid structures. *JCO* 2008;**26**:4410–7. https://doi.org/10.1200/JCO.2007.15.0284.
14. Herbst RS, Soria JC, Kowanetz M *et al.* Predictive correlates of response to the anti-PD-L1 antibody MPDL3280A in cancer patients. *Nature* 2014;**515**:563–7. https://doi.org/10.1038/nature14011.
15. Vanhersecke L, Brunet M, Guégan JP *et al.* Mature tertiary lymphoid structures predict immune checkpoint inhibitor efficacy in solid tumors independently of PD-L1 expression. *Nat Cancer* 2021;**2**:794–802. https://doi.org/10.1038/s43018-021-00232-6.

16. Graham DM, Appelman HD. Crohn's-like lymphoid reaction and colorectal carcinoma: a potential histologic prognosticator. *Mod Pathol Off J U S Can Acad Pathol Inc* 1990;**3**:332–5.
17. Buckowitz A, Knaebel HP, Benner A *et al.* Microsatellite instability in colorectal cancer is associated with local lymphocyte infiltration and low frequency of distant metastases. *Br J Cancer* 2005;**92**:1746–53. https://doi.org/10.1038/sj.bjc.6602534.
18. Ueno H, Hashiguchi Y, Shimazaki H *et al.* Objective criteria for Crohn-like lymphoid reaction in colorectal cancer. *Am J Clin Pathol* 2013;**139**:434–41. https://doi.org/10.1309/AJCPWHUEFTGBWKE4.
19. Väyrynen JP, Sajanti SA, Klintrup K *et al.* Characteristics and significance of colorectal cancer associated lymphoid reaction: Colorectal cancer associated lymphoid reaction. *Intl Journal of Cancer* 2014;**134**:2126–35. https://doi.org/10.1002/ijc.28533.
20. Zhao M, Yao S, Li Z *et al.* The Crohn's-like lymphoid reaction density: a new artificial intelligence quantified prognostic immune index in colon cancer. *Cancer Immunol Immunother* 2022;**71**:1221–31. https://doi.org/10.1007/s00262-021-03079-z.
21. Xu Z, Li Y, Wang Y *et al.* A deep learning quantified stroma-immune score to predict survival of patients with stage II–III colorectal cancer. *Cancer Cell Int* 2021;**21**:585. https://doi.org/10.1186/s12935-021-02297-w.
22. Ye Y, Wu X, Wang H *et al.* Artificial intelligence-assisted analysis for tumor-immune interaction within the invasive margin of colorectal cancer. *Ann Med* 2023;**55**:2215541. https://doi.org/10.1080/07853890.2023.2215541.
23. Kather JN, Krisam J, Charoentong P *et al.* Predicting survival from colorectal cancer histology slides using deep learning: A retrospective multicenter study. *PLoS Med* 2019;**16**:e1002730. https://doi.org/10.1371/journal.pmed.1002730.
24. Rakaee M, Kilvaer TK, Jamaly S *et al.* Tertiary lymphoid structure score: a promising approach to refine the TNM staging in resected non-small cell lung cancer. *Br J Cancer* 2021;**124**:1680–9. https://doi.org/10.1038/s41416-021-01307-y.
25. Maoz A, Dennis M, Greenson JK. The Crohn's-like lymphoid reaction to colorectal cancer-Tertiary lymphoid structures with immunologic and potentially therapeutic relevance in colorectal cancer. *Front Immunol* 2019;**10**:1884. https://doi.org/10.3389/fimmu.2019.01884.
26. Barmpoutis P, Di Capite M, Kayhanian H *et al.* Tertiary lymphoid structures (TLS) identification and density assessment on H&E-stained digital slides of lung cancer. *PLoS One* 2021;**16**:e0256907. https://doi.org/10.1371/journal.pone.0256907.
27. Di Caro G, Bergomas F, Grizzi F *et al.* Occurrence of tertiary lymphoid tissue is associated with T-cell infiltration and predicts better prognosis in early-stage colorectal cancers. *Clin Cancer Res Off J Am Assoc Cancer Res* 2014;**20**:2147–58. https://doi.org/10.1158/1078-0432.CCR-13-2590.
28. Peske JD, Thompson ED, Gemta L *et al.* Effector lymphocyte-induced lymph node-like vasculature enables naive T-cell entry into tumours and enhanced anti-tumour immunity. *Nat Commun* 2015;**6**:7114. https://doi.org/10.1038/ncomms8114.
29. Reticker-Flynn NE, Zhang W, Belk JA *et al.* Lymph node colonization induces tumor-immune tolerance to promote distant metastasis. *Cell* 2022;**185**:1924–42..https://doi.org/10.1016/j.cell.2022.04.019.
30. Yang J, Lu Z, Li L *et al.* Relationship of lymphovascular invasion with lymph node metastasis and prognosis in superficial esophageal carcinoma: systematic review and meta-analysis. *BMC Cancer* 2020;**20**:176. https://doi.org/10.1186/s12885-020-6656-3.
31. Petitprez F, de Reyniès A, Keung EZ *et al.* B cells are associated with survival and immunotherapy response in sarcoma. *Nature* 2020;**577**:556–60. https://doi.org/10.1038/s41586-019-1906-8.
32. Cabrita R, Lauss M, Sanna A *et al.* Tertiary lymphoid structures improve immunotherapy and survival in melanoma. *Nature* 2020;**577**:561–5. https://doi.org/10.1038/s41586-019-1914-8.
33. Posch F, Silina K, Leibl S *et al.* Maturation of tertiary lymphoid structures and recurrence of stage II and III colorectal cancer. *Oncoimmunology* 2018;**7**:e1378844. https://doi.org/10.1080/2162402X.2017.1378844.
34. Jenkins MA, Hayashi S, O'Shea AM *et al.* Pathology features in Bethesda guidelines predict colorectal cancer microsatellite instability: a population-based study. *Gastroenterology* 2007;**133**:48–56. https://doi.org/10.1053/j.gastro.2007.04.044.
35. Alexander J, Watanabe T, Wu TT *et al.* Histopathological identification of colon cancer with microsatellite instability. *Am J Pathol* 2001;**158**:527–35. https://doi.org/10.1016/S0002-9440(10)63994-6.
36. Morad G, Helmink BA, Sharma P *et al.* Hallmarks of response, resistance, and toxicity to immune checkpoint blockade. *Cell* 2021;**184**:5309–37. https://doi.org/10.1016/j.cell.2021.09.020.
37. Gunter MJ, Alhomoud S, Arnold M *et al.* Meeting report from the joint IARC-NCI international cancer seminar series: a focus on colorectal cancer. *Ann Oncol* 2019;**30**:510–9. https://doi.org/10.1093/annonc/mdz044.
38. Ganesh K, Stadler ZK, Cercek A *et al.* Immunotherapy in colorectal cancer: rationale, challenges and potential. *Nat Rev Gastroenterol Hepatol* 2019;**16**:361–75. https://doi.org/10.1038/s41575-019-0126-x.
39. Narayanan S, Kawaguchi T, Yan L *et al.* Cytolytic activity score to assess anticancer immunity in colorectal cancer. *Ann Surg Oncol* 2018;**25**:2323–31. https://doi.org/10.1245/s10434-018-6506-6.
40. Chen S, Song D, Chen L *et al.* Artificial intelligence-based non-invasive tumor segmentation, grade stratification and prognosis prediction for clear-cell renal-cell carcinoma. *Precis Clin Med* 2023;**6**:pbad019. https://doi.org/10.1093/pcmedi/pbad019.
41. Wang Z, Lin R, Li Y *et al.* Deep learning-based multi-modal data integration enhancing breast cancer disease-free survival prediction. *Precis Clin Med* 2024;**7**:pbae012. https://doi.org/10.1093/pcmedi/pbae012.

Received 11 September 2024; revised 28 September 2024; accepted 15 October 2024. published 18 October 2024